PV Panel to PV Panel Transfer Method for Modular Differential Power Processing

Chang Liu, *Student Member, IEEE*, Yue Zheng, *Student Member, IEEE*, and Brad Lehman, *Fellow, IEEE*

***Abstract*—This article proposes a realization of the photovoltaic (PV) panel to PV panel (P2P) method for the modular differential power processing (mDPP). The approach is modular and permits panels to be added to or removed from either series strings or paralleled connections. A voltage inner loop and power outer loop control strategy tracks the individual maximum power point of the PV panel, as well as converts only the differential power. The proposed method decouples the control loop performance of each PV module, making design simple. Simulation results validate the plug and play function for scalable PV system and MPPT accuracy. Hardware prototype is also built, and both indoor and outdoor experiments are provided to exhibit the advantage of this P2P method. Drawbacks and limitations are also discussed.**

***Index Terms*—Differential power processing (DPP), maximum power point, plug and play, solar energy, modular.**

I. Introduction

IN LARGE photovoltaic (PV) systems, maximum power point tracking (MPPT) is often performed with a centralized power converter [1], [2]. In this approach, PV panels are connected in series as a string, and then multiple series strings are connected in parallel through the combiner box. The output of the series–parallel connection becomes the input of the centralized MPPT converter, which is often an inverter for the ac output [3]–[5]. The approach is low cost and has high reliability.

In recent years, with the drastic price reduction of the solar panels, a new trend has emerged: solar panels and strings are beginning to be added to increase the capacity of older PV installations. Sometimes, there is not even an update on the capacity of the inverter, so it is just the dc capacity that is increased. However, this practice results in a new loss of energy because the old PV panels might not have similar performance characteristics as the new, more efficient panels. This mismatch can become even more apparent when the older PV panels have manufacturing variation, aging degradation, silicon impurities, dust accumulation or even might have partial shading [6]. All these factors will influence adjacent PV panel performance and may even by limit the total energy generation.

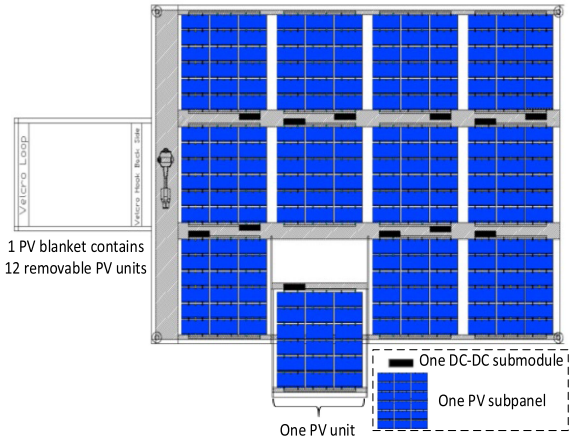

Fig. 1. "Solar blanket:" A modular solar panel concept with plug and play first proposed with *distributed* MPPT in [7] and [8].

In contrast of the central converter method, distributed maximum power point tracker (dMPPT) method has been proposed to mitigate any power mismatch problems [7], [8].

Each PV panel has its own converter and distributed controller to perform MPPT and deliver the power to the voltage bus [8]. Degradation of each PV panel will only influence its own MPP, and the partial shading effect will only lower the power output of those shaded PV panel. Other than this advantage, the dMPPT method also has modularity. PV panels can be added to an existing installation, or as in the papers [7], [8], an individual panel can be composed of modular subpanels, each with its own maximum power point tracker as in Fig. 1. Then, the subpanels can be slid in and out of a "blanket" to increase or decrease the PV power of the panel, without influencing each other submodules' performance, while using plug and play function in Fig. 1.

In both these above methods, the converters are designed based on full power processing (FPP) of the PV panel or subpanel that it is connected to. That is, the converter processes all the power generated by the source and delivers this entire power to the load. Given the assumption that the power loss is proportional to the power processed by the converter, the system efficiency is limited by the converter efficiency. Meanwhile, the dc–dc converter in Fig. 1 is introduced to boost up the subpanel's

Manuscript received March 1, 2021; revised June 8, 2021 and September 2, 2021; accepted October 2, 2021. Date of publication October 27, 2021; date of current version December 31, 2021. This paper was presented in part at the IEEE 18th Workshop on Control and Modeling for Power Electronics, Stanford University, Stanford, CA, USA, Jul. 9–12, 2017 and also presented in part at the IEEE Applied Power Electronics Conference and Exposition, Henry B. González Convention Center, San Antonio, TX, USA, Mar. 4–8, 2018. Recommended for publication by Associate Editor J. Popovic-Gerber. *(Corresponding author: Yue Zheng.)*

The authors are with the Department of Electrical and Computer Engineering, Northeastern University, Boston, MA 02115 USA (e-mail: liuchang199310@hotmail.com; zheng.yue@northeastern.edu; lehman@ece.neu.edu).

Color versions of one or more figures in this article are available at https://doi.org/10.1109/TPEL.2021.3123450.

Digital Object Identifier 10.1109/TPEL.2021.3123450

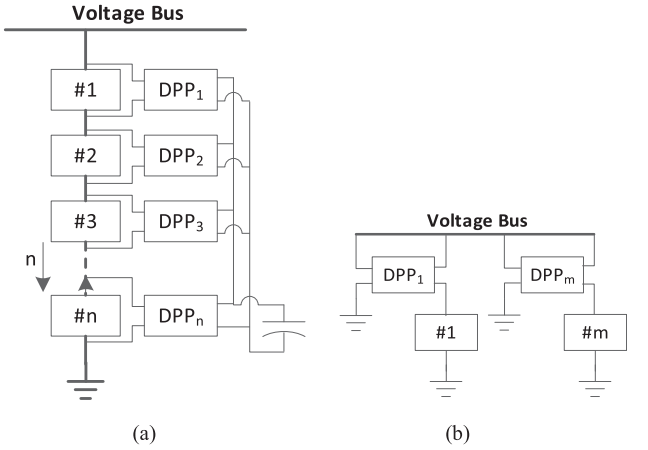

Fig. 2. DPP with different connections. (a) DPP in series connection. (b) DPP in parallel connection.

voltage to the bus voltage which leads to a high voltage gain but may also add certain extra power loss [11]–[13].

As an alternative, differential power processing (DPP) can be applied to a PV system [14]–[16] in order to improve the efficiency. In this approach only the mismatched power from the PV sources is processed through the converter. Most of the power is instead processed directly through the wire connections between the PV panels. By converting only a small part of the power, the total power loss is constrained to a lower level, which means a higher overall efficiency. From our preliminary conference result, numeral example from [10] shows the DPP system has ∼7% efficiency boost with nearly same converter than the traditional dMPPT system for the solar blanket in Fig. 1.

There are generally two approaches to DPP, classified as series DPP (sDPP) in Fig. 2(a) and parallel DPP (pDPP) in Fig. 2(b). More specifically, Fig. 2(a) shows the sDPP method with panel to virtual bus transfer [17]–[20] as an example, while neighbor to neighbor transfer method is presented in [21]–[25] and panel to bus method in [23] and [26]–[28] have also been proposed. A multiport ac coupled DPP example is also presented in [29] to address series-stacked power delivery problem to improve the efficiency in data storage server.

In Fig. 2(a), differential power is processed to or from each PV panel to the virtual bus created by adding the external series string capacitor. Because only small amounts of power are processed, DPP is feasible to be embedded in power management integrated circuit (PMIC) design for the cell level DPP function [30]. Under certain power converter rating limitation, a power-limited DPP converter [31] becomes more feasible for mismatched PV system.

Besides the higher efficiency, the DPP solution mentioned above also enjoys many other advantages, such as low-power switch rating, smaller DPP converter size and reliability enhancement. Unfortunately, these approaches have difficulties with scalability. Typically, a string of sDPP as in Fig. 2(a), cannot easily be connected in parallel to another group of sDPP. The voltage of each sDPP is the sum of each PV subpanel voltage at its MPP, which is different from other strings. Paralleling operation will clamp the voltage of all the strings, and force the

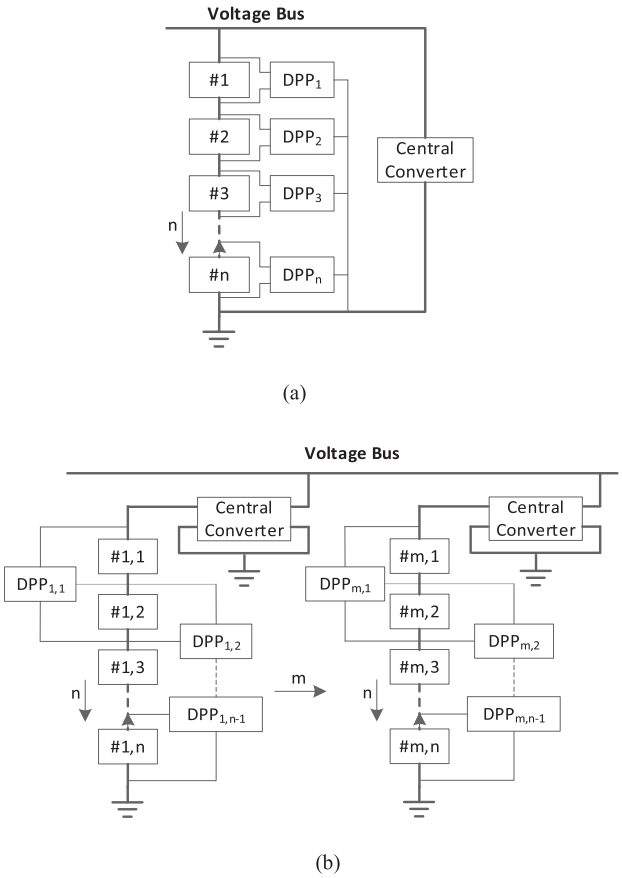

Fig. 3. DPP in series connection with central converter. (a) PV to the series string. (b) PV to PV.

PV strings to work away from MPP and produce less power. Similarly, pDPP, such as in Fig. 2(b), cannot effectively have PV panels connected in series. Fig. 3 illustrates two recently proposed sDPP structure with central converters (sDPPcc) and improved modularity [21], [32]–[35]. Since the central converter is indispensable for the MPPT function, the PV power is processed via dual stages. Processing full power of the PV system, central converter usually pays for the penalty of extra power loss and system cost. Furthermore, communication is required to improve the system dynamic performance, and this adds difficulty when scaling PV system or adding new PV panel to existed PV system.

This article proposes a modular differential power processing (mDPP) concept to help solve the modularity and scalability problem. A modular solar PV system is defined as a PV system where PV modules can be removed, replaced or added to the existing installation in either series or parallel configuration. To meet this design criteria, mDPP system architecture is proposed to have MPPT function in each DPP block and avoid the requirement of central converter (with a limitation in Section V). This concept yields the high levels of system efficiency and plug and play function [9], [10] in Fig. 4. To solve the complexity of previous hardware and firmware design, the distributed controller enables the plug and play function and simplifies the wire connection by avoiding communication

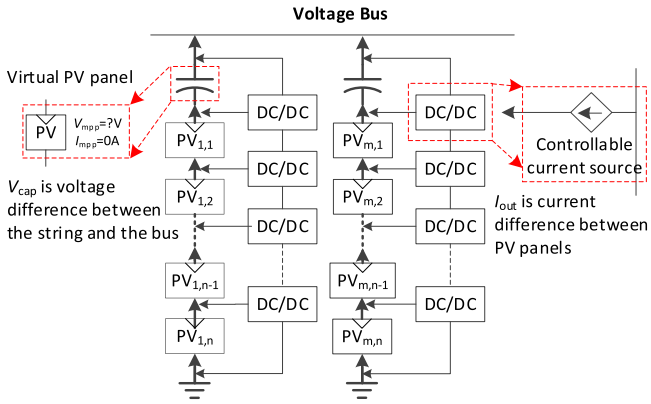

Fig. 4. Proposed mDPP diagram.

between converters. Each mDPP converter module has the same hardware configuration and software implementation, which could be installed for every PV panel in the PV array without any modification as the previous dMPPT method [7], [8]. Benefits of the proposed approach also include: a central converter is no longer needed for MPPT, which is typical of other DPP methods [36]–[38].

A drawback of the approach is that the top converter of the proposed mDPP system will not be working at DPP status (as mentioned in [39] and [40]). However, all the other converters in its series string work in DPP. The top converter only processes a fraction of the PV series string voltage. Therefore, even with the need to carry full current for the series capacitor, substantial efficiency improvements can be achieved, as the simulations and experiments demonstrate. This is different from the central converter traditional approach in Fig. 3(b), whose input voltage is the entire PV string voltage, meaning that it may process substantially higher input power, which can have higher power losses. Furthermore, the virtual PV panel in Fig. 4 plays an important role in solving the modularity and scalability problem.

Communication and data sharing between PV modules is eliminated. Instead a distributed controller is proposed. This enables the modular plug and play capability and simplifies seven connection wires in the previous solution [21] to only three wires per module.

The rest of this article is organized as follows. Architecture and topology of the mDPP method is introduced in Section II. The challenge and proposed control strategy are presented in Section III. The detailed mathematic model and steady state analysis of the inner control loop is discussed in Section IV. The converter power rating discussion is in Section V. Simulation is provided in Section VI. Hardware implementation and experiment verification is performed in Section VII. Finally, Section VIII concludes this article.

II. Introduction on Modular Differential Processing

A. Differential Power Processing

It is sometimes required to increase PV system size from both series and parallel connection. The traditional sDPP can compensate the differential current as a controllable current source to expand the system in series connection. On the other hand, the pDPP can provide the differential voltage between the strings or between the string and the bus to extend paralleled branch for the system. Meanwhile modularity requires the uniformity of every submodule for the system. A mDPP structure is proposed to obtain the scalability of the system and modularity as seen in Fig. 4. This approach combines the sDPP and pDPP and can be implemented by various topologies, two of which are described as follows.

For mDPP, each PV series string has an additional series capacitor that compensates the mismatch of voltages when connected in parallel with another string or to a voltage bus. It allows each PV panel to work at its own MPP when the sum of PV panels' voltage differs from the bus voltage. Hence, it is possible to scale the mDPP system by paralleling strings without clamping each other and losing energy. In the steady state, the voltage of each string will be fixed; therefore, the voltage difference between the bus and total PV panels is fixed. The capacitor voltage remains constant in steady state so that the average capacitor current is zero.

From the steady-state point of view, the capacitor works as absence of a PV panel in the string. Similar with other PV panels in the series, this capacitor acts as a "virtual PV panel," With the help of mDPP, this capacitor can hold differential voltage. In the previous serious DPP method, the central converter is required to compensate the voltage difference between the PV string and the voltage bus [32], [33]. The central converter usually reduces the system power loss and requires high power rating since the central converter is designed for full power.

The string current will flow in the direction illustrated in Fig. 4. Meanwhile, the mDPP structure will force the differential power to go through the DPP blocks in Fig. 4. With the help of mDPP, the PV modules can be connected in series to build up the voltage, yet maintain the maximum power output of the individual PV solar cell strings. Since PV panels in series will share the same string current, mDPP converter works as a controllable current source for each intermediate node between panels, including the virtual panel. By providing separate paths for the differential current and the string current, the differential power can be transferred by either of two proposed approaches: PV panel to "virtual" panel or PV panel to adjacent PV panel.

B. PV Panel to Virtual PV Panel (P2VP) Transfer (see Fig. 5)

Differential power can be transferred directly to the series capacitor, which is termed the virtual PV panel. The bidirectional converter will be used for DPP function since differential power can flow either from the PV panel to the capacitor or in the other direction. No common ground is shared by the PV panels. Therefore, isolation is further required for this application.

The P2VP approach is shown in Fig. 5 with a dual active bridge for the mDPP structure [9], which is extended in [41]. When the ith PV panel works at its maximum power point (MPP), the voltage and current are denoted as $V_{i,\mathrm{mpp}}$ and $I_{i,\mathrm{mpp}}$, with power $P_{i,\mathrm{mpp}}$.

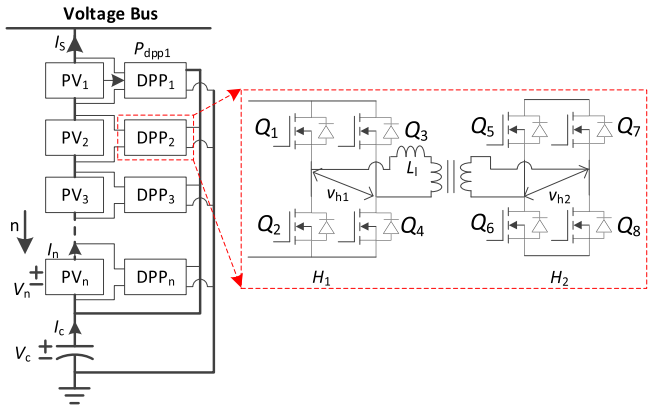

Fig. 5. Possible P2VP method for mDPP. This article focuses, although, on the P2P method in Fig. 6.

This means

$$\begin{aligned} I_i &= I_{i,\mathrm{mpp}} \\ V_i &= V_{i,\mathrm{mpp}} \\ (\forall i &\in \{1,2,3,\ldots,n\}). \end{aligned} \tag{1}$$

The differential power is transferred from each PV panel to the series capacitor directly which serves as an energy buffer as well as a voltage balancer. Similar to PV-to-bus method in [42], the power through P2VP transfer can be expressed as (2) by the assumption of no current limitation. $V_i \times (I_{i,\mathrm{mpp}} - I_s)$ is defined as the differential power to be extracted from the individual PV panel to make each PV panel work at its own MPP because this amount of power can adjust the current through the PV panel from string current I_s to its MPP current, $I_{i,\mathrm{mpp}}$. Note here the power through the converter $P_{\mathrm{dpp}\,i}$ is the same as the differential power

$$P_{\mathrm{dpp}i} = V_i \times (I_{i,\mathrm{mpp}} - I_s). \tag{2}$$

In steady state, the voltage across the capacitor keeps constant and the average current through the capacitor is zero. Applying Kirchhoff's current law (KCL) and Kirchhoff's voltage law (KVL) equations to the negative terminal of the capacitor, then (3) could be derived steady state as

$$\begin{aligned} I_c &= 0 \\ V_c &= V_{\mathrm{bus}} - \sum_{i=1}^{n} V_i. \end{aligned} \tag{3}$$

The capacitor has zero average power flow through it as

$$\begin{aligned} P_{\mathrm{cap}} &= \sum_{i=1}^{n} P_{\mathrm{dpp}i} - V_c \times I_s = 0 \\ &= \sum_{i=1}^{n} (V_i \times I_{i,\mathrm{mpp}}) - \sum_{i=1}^{n} V_i \times I_s - \left(V_{bus} - \sum_{i=1}^{n} V_i \right) \times I_s. \end{aligned} \tag{4}$$

Simplifying (4), (5) can be derived as

$$V_{\mathrm{bus}} \times I_s = \sum_{i=1}^{n} P_{i,\mathrm{mpp}}. \tag{5}$$

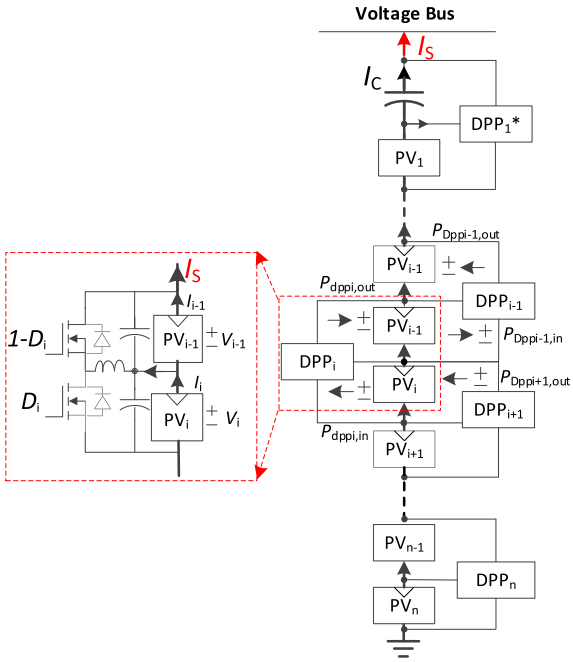

Fig. 6. Proposed P2P Method for mDPP. The top converter DPP_1^* processes full string current and the differential voltages between PV string voltages and bus voltage in paralleled strings. All other converters process the differential currents between the series PV modules.

From (5), the string power is the sum of each PV panel's maximum power. Furthermore, the PV string voltage is allowed to be different from the bus voltage or other voltage strings. Therefore, the proposed mDPP structure now allows different PV strings to be placed in parallel since the strings no longer clamp the voltage of each other. This explains the scalability of the system. The capacitor compensates for the voltage difference in the steady state.

C. PV Panel to PV Panel (P2P) Transfer (see Fig. 6)

Alternatively, modular differential power can also be transferred between adjacent PV modules using the bidirectional buck–boost converter instead of transferring the power from PV panel to the series capacitor in the P2VP method described above. This P2P transfer approach extends the architecture presented in [33] to consist of n converters instead of $(n-1)$, where n is the number of PV modules per string. The schematic for the P2P transfer structure is shown in Fig. 6, where only one string is shown, although there are no restrictions on adding more PV panels. The voltage bus is accessible to paralleling more branches.

The duty ratio for DPP_i converter D_i and its complimentary duty ratio, $D_i^{'} = 1 - D_i$, is generated for the synchronized buck-boost converter by a distributed controller. The duty ratio is adjusted to regulate the power of each PV panel to its maximum power. The bidirectional buck–boost converter has the ideal relationship for Fig. 6 as

$$\frac{V_i}{V_{i-1}} = \frac{D_i'}{D_i} = \frac{1 - D_i}{D_i}. \tag{6}$$

Every P2P transfer structure will deliver the certain power from one PV panel to the former series PV panel.

As the result, the power of each mDPP model $P_{\mathrm{dpp}i,\mathrm{in}}$, is related to its previous one, $P_{\mathrm{dpp}i+1,\mathrm{out}}$, which introduces coupling effect and adds complexity to the distributed controller design.

Assuming 100% efficiency with $P_{\mathrm{dpp}i,\mathrm{in}} = P_{\mathrm{dpp}i,\mathrm{out}}$, the DPP_i in Fig. 6 will be processing power flow from and to DPP_{i+1} and the differential power from $\mathrm{PV_i}$. The power through the converter $P_{\mathrm{dpp}i}$ contains 2 parts in (7), the differential power for the ith PV panel and the power from (i+1)th DPP module

$$P_{\mathrm{dpp}i,\mathrm{in}} = V_i \times (I_{i,\mathrm{mpp}} - I_s) + P_{\mathrm{dpp}i+1,\mathrm{out}}. \tag{7}$$

Applying (7) to all the mDPP modules leads to the following:

$$\begin{aligned}
P_{\mathrm{dpp1,in}} &= V_1 \times (I_{1,\mathrm{mpp}} - I_s) + P_{\mathrm{dpp2,out}} \\
P_{\mathrm{dpp2,in}} &= V_2 \times (I_{2,\mathrm{mpp}} - I_s) + P_{\mathrm{dpp3,out}} \\
&\cdots \\
P_{\mathrm{dppi,in}} &= V_i \times (I_{i,\mathrm{mpp}} - I_s) + P_{\mathrm{dpp}i+1,\mathrm{out}} \\
&\cdots \\
P_{\mathrm{dpp}n,\mathrm{in}} &= V_n \times (I_{n,\mathrm{mpp}} - I_s).
\end{aligned} \tag{8}$$

Since $P_{\mathrm{dpp}i,\mathrm{in}} = P_{\mathrm{dpp}i,\mathrm{out}}$, combining the equations in (8) leads to

$$\begin{aligned}
P_{\mathrm{dpp1,in}} &= \sum_{i=1}^{n} V_i \times (I_{i,\mathrm{mpp}} - I_s) \\
&= \sum_{i=1}^{n} P_{i,\mathrm{mppt}} - I_s \times \sum_{i=1}^{n} V_i.
\end{aligned} \tag{9}$$

In steady state, the capacitor voltage is fixed as the voltage difference between the bus and total PV panels and has zero average current through it as in (3). The steady state dc output current of the first DPP module is the string current, thus

$$P_{\mathrm{ddp1,out}} = V_C \times I_s. \tag{10}$$

Considering (9) and (10), the output power of the string can be calculated as

$$\begin{aligned}
V_C \times I_s &= \sum_{i=1}^{n} P_{i,\mathrm{mppt}} - I_s \times \sum_{i=1}^{n} V_i \\
\sum_{i=1}^{n} P_{i,\mathrm{mppt}} &= \left(\sum_{i=1}^{n} V_i + V_C \right) \times I_s = V_{\mathrm{bus}} \times I_s.
\end{aligned} \tag{11}$$

which is the same form as (5), although different system connection is used. This P2P connection inherits two benefits: the output power of the string is the sum of the maximum power of each PV panel; and PV string voltage can be different from the voltage bus or other PV string, which enables the paralleling of more PV strings. Furthermore, the converter used in P2P method does not require isolation which may bring benefit to the efficiency, material cost and reliability considerations.

In order to realize the easy plug and play function, the connection wires of P2P is much less than that of P2VP. The converter of P2P has half of the FET number and do not need coupling coils, which decrease the BOM cost. The PV2P topology might suit for other applications, but P2P is more suitable for modular PV systems. Therefore, the following discussion are mainly focused on P2P.

III. Control Strategy for PV Panel to PV Panel Transfer

One of the more difficult challenges in DPP for solar PV panels is that the coupling of the controllers of the individual PV panel make it more difficult to achieve stable performance at MPPT. Sometimes, global optimization or nonlinear controllers may need to be used [35], [36]. Considering that the approach in this article introduces an additional virtual bus (capacitor) for improved modularity, it is vital to present a control approach that can regulate each subpanel to operate at MPP while guaranteeing stability. Specifically, this section and Section IV demonstrate that it is possible to design simple proportional–integral (PI) controllers in a distributed fashion for the proposed P2P architecture of the mDPP method.

A. Mathematical Model and Control Challenge

A bidirectional buck–boost converter between two PV panels is used for mDPP converter in Fig. 6. The differential current between the PV panel $I_{\mathrm{PV}i}$ and the string current I_{s} leads to differential power. This differential power is processed from one PV panel to its next PV panel sequentially. The top converter, DPP_1 in Fig. 6, processes the differential power to the virtual PV panel, the series capacitor. During the steady state operation, the differential power flows to the voltage bus instead of charging the series capacitor. The virtual PV panel compensates the voltage difference between the PV strings and the voltage bus. The detailed power flow of each PV panel and mDPP converter is illustrated in our preliminary conference paper [9].

The low side switch of the bidirectional buck–boost converter has a duty ratio of d_i while the high side switch is controlled by the complementary duty ratio of (1-d_i). The voltage between the two terminals of the converter is defined in the Fig. 6 as $v_{\mathrm{PV}i\text{-}1}$ and $v_{\mathrm{PV}i}$, respectively. A total number of n PV panels are connected in series in each string. $d_i(t)$ is slowly adjusted discretely by the microcontroller. On this slow time scale with fast enough inner-loop controller, the mathematical model for the buck–boost converter can be simplified as

$$\frac{v_{\mathrm{PV}i}(t)}{v_{\mathrm{PV}i-1}(t)} = \frac{1 - d_i(t)}{d_i(t)} (i \in 1, 2, 3, \ldots, N). \tag{12}$$

Voltage across the virtual PV panel is defined as v_c. As there is a P2P converter between every two panels, including the virtual PV panel, the voltage across the ith PV panel can be calculated as

$$v_{\mathrm{PV}i}(t) = v_c(t) \times \prod_{j=1}^{i} \frac{1 - d_j(t)}{d_j(t)}. \tag{13}$$

The voltage bus is regulated by external circuit, i.e. battery backup system or grid tie inverter, which can be considered to have a relatively constant voltage of V_{bus}. The sum of each PV

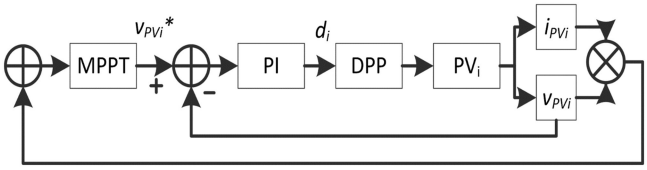

Fig. 7. Control diagram of power outer loop and current inner loop.

panel including the virtual PV panel equals to the bus voltage in

$$V_{\text{bus}} = v_c(t) + \sum v_{\text{PV}i}(t) = v_c(t) \times \left(1 + \sum_{i=1}^{N} \prod_{j=1}^{i} \frac{1-d_j(t)}{d_j(t)}\right). \quad (14)$$

Combining (13) and (14), the voltage across the *i*th PV panel $v_{\text{PV}i}$ can be modified in

$$v_{\text{PV}i}(t) = V_{\text{bus}} \times \frac{\prod_{j=1}^{i} \frac{1-d_j(t)}{d_j(t)}}{(1 + \sum_{i=1}^{N} \prod_{j=1}^{i} \frac{1-d_j(t)}{d_j(t)})}. \quad (15)$$

Equation (15) shows that $v_{\text{PV}i}$ is a function of every duty ratio of the P2P converter in the same string. This is called the coupling effect because the control action of each mDPP module ($v_{\text{PV}i}$) is related not only with its control signal (d_i), but also control signals ($d_j, j{\neq}i$) of all other models.

Applying the traditional MPPT algorithm to this PV system is difficult because of this coupling effect [10]. The variation of the PV panel voltage is usually a function of a perturbed small signal duty ratio of a converter for the traditional MPPT. However, in this DPP structure, the duty ratio of each PV panel occurs in all the other PV panels in the same string. Advanced control algorithms [32], [33] have been proposed for sDPP structures that face the similar coupling effect. For example, it is possible to use Lagrange equations to decouple the control parameter. This approach relies on both local voltage sensing and communication between all the differential power converters in the same string. In particular, the communication requirement increases the system cost as well as may influence reliability [43]–[45]. Furthermore, the advanced controller may require an additional global MPPT converter that handles full power from the PV system. This may take away the advantage brought by DPP. One goal of this research is to introduce control approach that helps mitigate this coupling effect and is simple to implement a plug and play function.

B. Dual Loop Controller Design

To solve the problem of Section IV, a distributed MPPT control algorithm based on the P2P transfer structure is proposed. The proposed dual loop controller is designed to mitigate this coupling effect and track the individual maximum power point with only local information.

Power outer loop and voltage inner loop for the *i*th PV module are shown in the Fig. 7. The inner loop regulates the *i*th PV panel voltage, while the outer loop deals with its MPPT function. The MPPT block represents the controller of the outer loop. PI block is the controller for the inner loop and generates the duty ratio for its related P2P converter. The DPP block is the bidirectional buck–boost converter in the mDPP system and the PV block is each PV panel. As no communication is required, this control algorithm depends on only local voltage and current information, which enables the plug and play function.

The inner loop controller senses the local PV panel voltage v_{PVi} and generates duty ratio d_i from the PI controller. Power Outer loop is implemented by a voltage based MPPT controller. Perturb and observe (P&O) algorithm is used to seek for a reference voltage for *i*th PV panel $v^*_{\text{PV}i}$. And this voltage signal serves as the voltage reference of the voltage inner loop.

DPP method usually processes a small proportion of power. Thus, high frequency (hundreds of kilohertz) dc–dc converter with smaller volume is preferred. The speed of proposed voltage inner loop is around 1/10 or lower of switching frequency. Power outer loop is run much slower than the inner voltage loop so that the outer loop will adjust the voltage reference after the inner loop reaches its steady state and compensate the steady-state error. It is common for MPPT to have less than 1/100 of the inner voltage loop bandwidth.

Since modularity is required for the DPP method, each controller includes plug and play function.

IV. Stability and Steady-State Error

The cross-coupling effect can be further discussed through a mathematical model. Equations (12)–(15) are nonlinear in duty ratio, so linearization is applied. Assume that the duty ratio $d_i(t)$ consists of two parts: upper-case time-invariant dc term of D_i superimposed with the small signal term of $\hat{d}_i(t)$. Similar decomposition can be applied to the other variables

$$\begin{aligned} d_i(t) &= D_i + \hat{d}_i(t) \\ v^*_{\text{PV}i}(t) &= V^*_{\text{PV}i} + \hat{v}^*_{\text{PV}i}(t) \\ v_{\text{PV}i}(t) &= V_{\text{PV}i} + \hat{v}_{\text{PV}i}(t). \end{aligned} \quad (16)$$

And the duty ratio can also be formed in a vector as

$$\mathbf{d}(t) = \begin{bmatrix} d_1(t) \\ d_2(t) \\ \vdots \\ d_N(t) \end{bmatrix} \approx \mathbf{D} + \hat{\mathbf{d}}(t) = \begin{bmatrix} D_1 \\ D_2 \\ \vdots \\ D_N \end{bmatrix} + \begin{bmatrix} \hat{d}_1(t) \\ \hat{d}_2(t) \\ \vdots \\ \hat{d}_N(t) \end{bmatrix}. \quad (17)$$

For the *i*th PV panel, the voltage $v_{\text{PV}i}(t)$ is defined as

$$v_{\text{PV}i}(t) = f_i(\mathbf{d}(t)) = V_{\text{bus}} \times \frac{\prod_{j=1}^{i} \frac{1-d_j(t)}{d_j(t)}}{\left(1 + \sum_{i=1}^{N} \prod_{j=1}^{i} \frac{1-d_j(t)}{d_j(t)}\right)}. \quad (18)$$

Expanding the function f_i in a Taylor series and assuming the differential term is small enough, we can ignore higher order terms to obtain

$$f_i(\mathbf{D} + \hat{\mathbf{d}}(t)) = f(\mathbf{D}) + \sum_{j=1}^{N} \left(\frac{\partial f_i}{\partial d_j(t)}\bigg|_{\mathbf{D}} \times \hat{d}_j(t) \right) \quad (19)$$

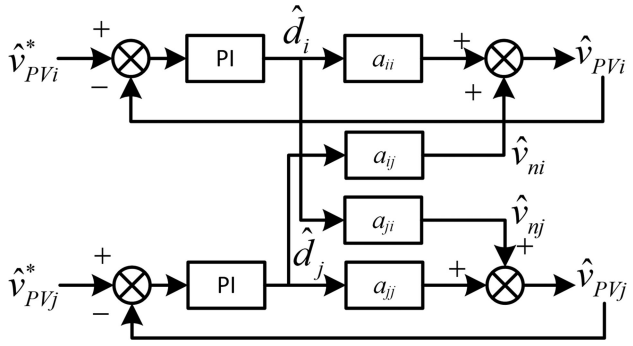

Fig. 8. Modular differential power processing diagram.

where the term $\frac{\partial f_i}{\partial d_j(t)}|_{\mathbf{D}}$ means the partial derivative of function f_i with respect to $d_j(t)$ and is evaluated at its steady-state value **D**, which is $\frac{\partial f_i}{\partial d_j(t)}|_{\mathbf{d}(t)=\mathbf{D}}$.

Under the steady-state analysis, we obtain $V_{PVi} = f_i(\mathbf{D})$. So that, (18) and (19) imply

$$\hat{v}_{\mathrm{PV}i}(t) = \sum_{j=1}^{N} \left.\frac{\partial f_i}{\partial d_j(t)}\right|_{\mathbf{D}} \times \hat{d}_j(t). \tag{20}$$

Define the partial derivative of function f_i to d_j(t) as

$$a_{ij} = \left.\frac{\partial f_i}{\partial \hat{d}_j(t)}\right|_{\mathbf{D}} \tag{21}$$

which represents the influence of *j*th duty ratio on the *i*th PV panel. $\hat{\mathbf{v}}(s)$represents the voltage of each PV panel in Laplace domain as

$$\begin{aligned}\hat{\mathbf{v}}(s) &= \begin{bmatrix} \hat{v}_{\mathrm{PV}1}(s) \\ \hat{v}_{\mathrm{PV}2}(s) \\ \vdots \\ \hat{v}_{\mathrm{PV}N}(s) \end{bmatrix} = \mathbf{A}\hat{\mathbf{d}}(s) \\ &= \begin{bmatrix} a_{11} & a_{12} & \cdots & a_{1N} \\ a_{21} & a_{22} & \cdots & a_{2N} \\ \vdots & \vdots & \ddots & \vdots \\ a_{N1} & a_{N2} & \cdots & a_{NN} \end{bmatrix} \begin{bmatrix} \hat{d}_1(s) \\ \hat{d}_2(s) \\ \vdots \\ \hat{d}_N(s) \end{bmatrix}. \end{aligned} \tag{22}$$

For each *i*th PV panel, each $j(j = 1, 2, \ldots, N, j \neq i)$ PV panel together with its mDPP converter has influence on $\hat{v}_{\mathrm{PV}i}(s)$ with the coupling effect term of a_{ij}. The transfer block diagram with voltage inner loop and coupling effect shows in Fig. 8. The upper loop represents the controller of the *i*th PV panel while the lower loop of the *j*th PV panel introduces the coupling effect to the *i*th PV panel. To simplify the diagram, only this coupling effect to the *i*th PV panel is shown here to represent $N - 1$ of coupling loop in the real system. Fig. 8 is valid for all DPP converter connection used in Fig. 6 regardless of converter topology itself. Different converter topology, i.e. buck–boost or isolated converter, only alters the cross-coupling effect term of a_{ij}.

The control to output transfer function shows as

$$G_{ii}(s) = \frac{\hat{v}_{\mathrm{PV}i}(s)}{\hat{v}^*_{\mathrm{PV}i}(s)} = \frac{a_{ii}(K_p + \frac{K_i}{s})}{1 + a_{ii}(K_p + \frac{K_i}{s})}. \tag{23}$$

Applying (23) to the *j*th loop, we can get

$$\hat{d}_j(s) = \frac{(K_p + \frac{K_i}{s})}{1 + a_{jj}(K_p + \frac{K_i}{s})} \times \hat{v}^*_{\mathrm{PV}j}(s). \tag{24}$$

Disturbance to output transfer function for the *i*th PV panel is calculated as

$$G_{\mathrm{in}}(s) = \frac{\hat{v}_{\mathrm{pv}i}(s)}{\hat{v}_{ni}(s)} = \frac{1}{1 + a_{ii}(K_p + \frac{K_i}{s})}. \tag{25}$$

So, the transfer function from *j*th PV panel reference to the *i*th PV panel voltage can be expressed as

$$\begin{aligned} G_{ij}(s) &= \frac{\hat{v}_{\mathrm{PV}i}(s)}{\hat{v}^*_{\mathrm{PV}j}(s)} = \frac{\hat{v}_{\mathrm{PV}i}(s)}{\hat{v}_{ni}(s)} \times \frac{\hat{v}_{ni}(s)}{\hat{d}_j(s)} \times \frac{\hat{d}_j(s)}{\hat{v}^*_{\mathrm{PV}j}(s)} \\ &= \frac{1}{1 + a_{ii}(K_p + \frac{K_i}{s})} \times \frac{a_{ij}(K_p + \frac{K_i}{s})}{1 + a_{jj}(K_p + \frac{K_i}{s})}. \end{aligned} \tag{26}$$

The response of each PV panel can be calculated as

$$\begin{aligned}\hat{\mathbf{v}}(s) &= \begin{bmatrix} \hat{v}_{\mathrm{PV}1}(s) \\ \hat{v}_{\mathrm{PV}2}(s) \\ \vdots \\ \hat{v}_{\mathrm{PV}N}(s) \end{bmatrix} = \mathbf{G}(s)\hat{\mathbf{v}}^*(s) \\ &= \begin{bmatrix} G_{11}(s) & G_{12}(s) & \cdots & G_{1N}(s) \\ G_{21}(s) & G_{22}(s) & \cdots & G_{2N}(s) \\ \vdots & \vdots & \ddots & \vdots \\ G_{N1}(s) & G_{N2}(s) & \cdots & G_{NN}(s) \end{bmatrix} \begin{bmatrix} \hat{v}^*_{\mathrm{PV}1}(s) \\ \hat{v}^*_{\mathrm{PV}2}(s) \\ \vdots \\ \hat{v}^*_{\mathrm{PV}N}(s) \end{bmatrix}. \end{aligned} \tag{27}$$

where **G(*s*)** is the transfer function matrix of $G_{ij}(s)$. The diagonal term has the expression as (23) while otherwise $G_{\mathrm{ij}}(s)$ can be calculated as (26), which also presents the cross-coupling effect from a transfer function point of view.

To maintain the local bounded-input bounded-output stability of the system, each transfer function $G_{ij}(s)$ must have all poles with negative real part. This occurs in (23) and (26) when the solution of

$$1 + a_{ii}(K_p + \frac{K_i}{s}) = 0 \,\forall i \in [1, 2, \ldots, N] \tag{27}$$

satisfies Re(s) < 0, or equivalently

$$s = -\frac{a_{ii}K_i}{1 + a_{ii}K_p} < 0. \tag{28}$$

The Appendix demonstrates that all $a_{ii} < 0$. Therefore, stability of the linearized system will be guaranteed provided that

$$\begin{aligned} K_i &> 0 \\ K_p &> \frac{1}{|a_{ii}|_{\min}}. \end{aligned} \tag{29}$$

Of course, the assumption in the controller derivation has been that loop gain crossover frequencies (or bandwidth) is

sufficiently below the natural resonant frequency of the converters. As we show in the simulations and experiments, this might typically have loop gains with crossover frequency in the 10s of Hz for typical systems, while the converters' natural resonant frequency is often 1000× higher. The gains should K_p and K_i are therefore small. Then each perturbation in duty ratio has enough time to lead to (12) being (approximately) valid.

Furthermore, it is easy to derive that the steady state error of the controller is zero, and the differential power controller can force operation at designed reference. If we assume a step reference

$$\hat{v}^*_{\mathrm{PV}i}(s) = \frac{|\hat{v}^*_{\mathrm{PV}i}|}{s}. \tag{30}$$

For the *i*th PV panel, the response can be divided into two parts. One comes from its own reference while the rest $N-1$ terms come from other PV panels as

$$\hat{v}_{\mathrm{PV}i}(s) = G_{ii}(s)\hat{v}^*_{\mathrm{PV}i}(s) + \sum_{j=1,j\neq i}^{N} G_{ij}(s)\hat{v}^*_{\mathrm{PV}j}(s). \tag{31}$$

Applying final value theorem to (20), the time domain response can be obtained as

$$\begin{aligned}\lim_{t\to\infty}\hat{v}_{\mathrm{PV}i}(t) &= \lim_{s\to 0} s\times\hat{v}_{\mathrm{PV}i}(s)\\ &= \lim_{s\to 0} s\left(G_{ii}(s)\frac{|\hat{v}^*_{\mathrm{PV}i}|}{s} + \sum_{j=1,j\neq i}^{N} G_{ij}(s)\frac{|\hat{v}^*_{\mathrm{PV}i}|}{s}\right).\end{aligned} \tag{32}$$

Noting that

$$\begin{cases}\lim_{s\to 0}\left(\frac{a_{ii}(K_p+\frac{K_i}{s})}{1+a_{ii}(K_p+\frac{K_i}{s})}\right)=1\\ \lim_{s\to 0}\left(\frac{1}{1+a_{ii}(K_p+\frac{K_i}{s})}\times\frac{a_{ij}(K_p+\frac{K_i}{s})}{1+a_{jj}(K_p+\frac{K_i}{s})}\right)=0.\end{cases} \tag{33}$$

Leads to

$$\lim_{t\to\infty}\hat{v}_{\mathrm{PV}i}(t) \approx 1\times|\hat{v}^*_{\mathrm{PV}i}| + \sum_{j=1,j\neq i}^{N} 0\times\left|\hat{v}^*_{\mathrm{PV}j}\right|. \tag{34}$$

This can be written in time domain matrix form as

$$\begin{aligned}\lim_{t\to\infty}\hat{\mathbf{v}}(t) &= \lim_{s\to 0}\mathbf{G}(s)\hat{\mathbf{v}}^*\\ &= \begin{bmatrix}1&0&\cdots&0\\0&1&\cdots&0\\\vdots&\vdots&\ddots&\vdots\\0&0&\cdots&1\end{bmatrix}\begin{bmatrix}\hat{v}^*_{\mathrm{PV1}}\\\hat{v}^*_{\mathrm{PV2}}\\\vdots\\\hat{v}^*_{\mathrm{PV}N}\end{bmatrix} = \mathbf{I}\hat{\mathbf{v}}^* = \hat{\mathbf{v}}^*.\end{aligned} \tag{35}$$

This demonstrates that the PI controller only requires local voltage and current measurement, and no information and prior knowledge of PV installation is required. From (35), the cross-coupling effect does not show up after PI control loop reaches its steady state with zero steady state. This analysis assumes the gains of the controller are selected so the real parts of the solution of (28) have Re(s) <0 and lie in open left half plane. The desired steady state will be achieved when the simple PI control rules are maintained. Therefore, if the MPPT changes its P&O increment sufficiently slower than the inner loop (see Fig. 7), each DPP$_i$ converter will reach its reference $V_{\mathrm{PV}i}$ steady-state voltage, as desired. Then, the individual PV currents Ii can be directly measured to compute the panels PV power $P_{\mathrm{PV}i}$. Because the steady-state coupling is mitigated, standard P&O algorithms are implemented, typical as more traditional (e.g. centralized converter) panels.

The advanced control algorithms in [32] and [33] are not needed, so it is possible to design simple and distributed firmware for each controller. The identical controller design makes the plug and play function possible. Of course, the controller design approach in this article sacrifices speed of response (becoming slower) in order to gain design simplicity. It also requires current sensors for each panel (which are not necessarily required in [33]). But only the individual voltage and current of the panels are required, with no communication between the DPP converters.

V. Converter Power Rating Considerations

Although topology and controller design can support full modularity of the proposed system level connection, practical effort on power rating should be given extra consideration to each converter when designing the PV system with proposed mDPP method. In this section, the power rating of each converter is mainly discussed in two aspects: PV panel/subpanel arrangement and tolerance to variation and fault condition.

Since we are designing a DPP system, the system should be designed to operate as a low state of imbalance at normal/typical condition. The imbalance of the PV system is mainly represented into two different subsets: the current difference between two series connected PV panels and the voltage difference between PV string voltages and bus voltage in paralleled strings. It is suggested to minimize the difference by having PV panels with similar MPP voltage and current in each string as well as similar string voltage across different strings. With the freedom of the plug and play feature, it is easy to rearrange the PV panel array to make such situation. Failing to do so might vanish the efficiency benefit brought by differential power process ideas. One extreme example is to setup 1 × 6V PV panel in parallel with 7 × 6V PV series submodules in a string. The DPP converter for that 1 × 6V PV panel has to take the full string voltage as well as the full string current and eventually process full power. This extreme configuration is opposite to our original design intention. With the freedom of plug and play and modularity design, the system can be reconfigured as a 4 × 6V PV panel string in parallel with another 4 × 6V PV panel string. In this case, the top converter would process any differential mismatch voltage between PV string voltages and bus voltage, and the DPP converters underneath it would process the mismatched series PV currents. When this flexibility to operate at the lower system bus voltage is allowed, very high efficiency can be achieved. In any case, it is reasonable to rate the components for the top converter at full rated string power, even though in normal circumstances it processes low power due to its purpose to equalizing differential voltages between PV string voltages and bus voltage.

It should also be noted that extreme shading difference on the lower panels has been shown to substantially increase the stress on the power converters, adding voltage stress as well as current stresses [46]. This is the same as in the proposed system. To handle these extreme cases in DPP systems, a designer may decide to rate each converter for full power. However, the approach in this article (simulations and experiments) is to not design completely for the extreme cases, but for the more common mismatch cases. For example, the converters in the both the simulation and experimental plug and play PV system in Sections V and VI are designed to handle ~2.2X module power, which means that two solar PV modules can be removed in a string and the PV string current can still be processed completely.

VI. Simulation Results

This section includes simulation results that validate the plug and play function as well as the stable and proper MPPT algorithm. Since ideal switching is used in the simulation, the power loss and parasitic effect are not concerned in this section and will be further discussed in the experimental part.

Fig. 9(a) shows the PV blanket with smaller PV panel in series and parallel connection.

At time $t = 0$, PV_1–PV_6 is installed in the PV blanked with 8 V/2 A rating. As shown in Box#1, there are three PV panels are connected in series and two PV strings are connected in parallel. Considering the aging effect [47], [48], a 10% of degradation with random value is given to each PV panel on their performance at MPP ($V_{\rm mpp}$, $I_{\rm mpp}$).

Then, different PV panels, PV_7–PV_{11} with 11 V/3 A rating is added to the existed installation with both series connection and parallel connection. Noted in box #2, PV_7 and PV_8 are added in series with previous PV string at time 2 s. At time 4 s, PV_9, PV_{10} and PV_{11} build the third string and are connected in parallel in box #3. Fig. 9(a) only shows the final connection of PV blanket for clearer schematic.

Fig. 9(b) shows one typical mDPP converter connected between adjacent PV panel. The proposed close loop control algorithm for one mDPP module is shown in Fig. 9(c). Note that each mDPP module measures only its local PV panel voltage and current and no information is shared between modules. Inner voltage loop consists of PI controller while outer MPPT loop is implemented in P&O method, respectively.

Fig. 10 shows the ideal maximum output power P_m and actual output power of the entire PV blanket $P_{\rm out}$. The ideal maximum output power is calculated as the sum of the maximum power of all the PV panels in the circuit. So, the ideal output power suddenly increases at the time when new PV panels are added. The actual output power is measured at the output of whole PV system. After some transient time after new PV panel is added, the actual output power reaches its ideal maximum power, which verifies the effectiveness of the MPPT function.

Fig. 10(b) shows the voltage across each PV panel. Note here the voltage shows 0 V for the new PV panel before it is added to the system. At time 2 s, the PV7 is connected in series with PV_1, PV_2, and PV_3, which influences the voltage of the other PV

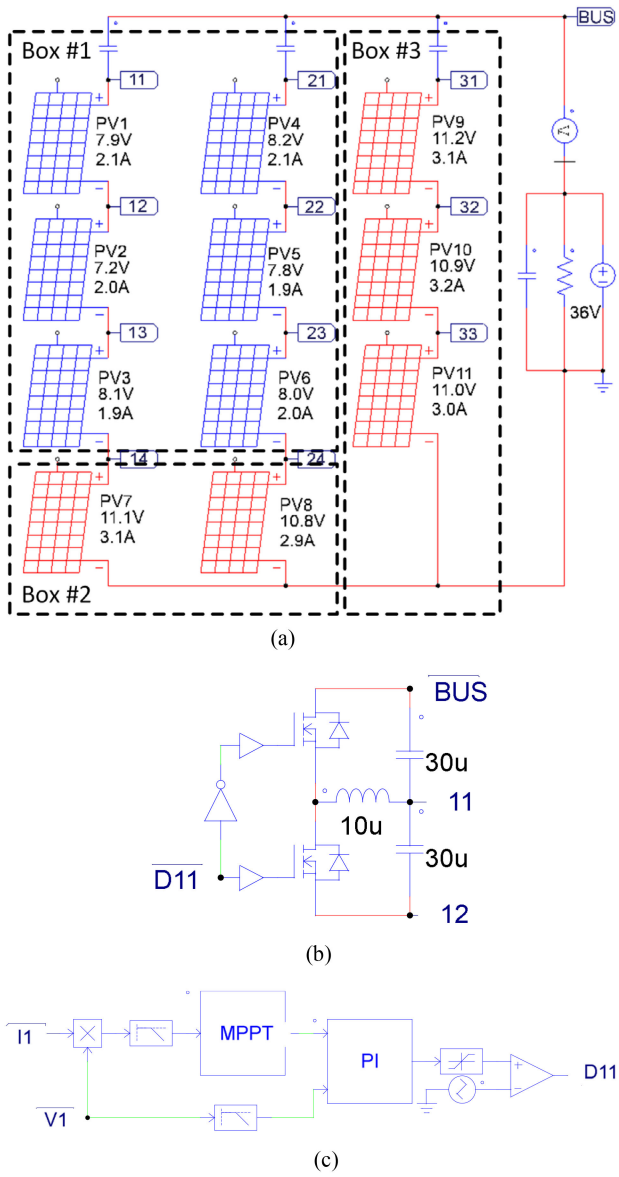

Fig. 9. Simulation schematic of a solar system in PSIM. (a) Simulation schematic of PV blanket. (b) P2P transfer converter for PV_1. (c) Distributed controller for PV_1.

panels due to the coupling effect. But after duty ratio adjustments of each mDPP converter, each voltage settles to its MPP voltage.

At time 4 s, new PV string is added to the system and does not impact other existing PV units. Later on, PV_9, PV_{10}, and PV_{11} reach its own MPP state.

The simulations also demonstrate important behavior for the following.

1) When new PV panels are added in the same PV system, it normally causes some PV panels to operate away from their MPP until a proper compensation is provided.
2) During transient period, each PV panel's voltage is changing because they are tightly coupled in the same PV string through converters. After transient time, the changes due to adding PV panel is compensated by changing the

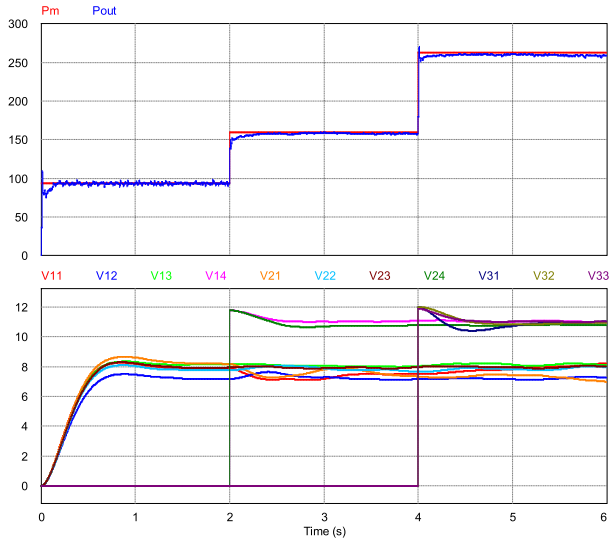

Fig. 10. Startup waveform of power of each PV panel.

duty cycle in the closed loop control scheme. All the PV modules are able to reach MPP finally.

3) The virtual bus (series capacitor) is only used to absorb the small voltage mismatch between the strings, so the top converter has benefits that might also lead to lower power losses. For instance, notice that in the simulation example (see Fig. 9), each of the virtual bus capacitors may have only 0.2–2 V across it. This may lead to a design selection of lower loss switches because of possible reduced voltage ratings, but it should always lead to some reduction in switch commutation power losses (for fair comparison, though, to the distributed power processing architectures, we kept all switch ratings the same—and still successfully validated the improved system level efficiency).

This simulation verifies the coupling effect can be eliminated after several control duty ratio steps by each individual distributed controllers.

VII. Experimental Results

This section is divided into four parts. First, modular DPP structure is introduced to have simplified wire connection compared with existed method. Then, indoor experiments verify the MPPT function of proposed method. Furthermore, outdoor experiments validate the performance of the system under real world shading effects. Finally, plug and play experiments show the benefit of easy installation.

A. mDPP Hardware Design

PV panels normally have a junction box on their back side where usually the bypass diodes are installed. Therefore, it is possible to merge the mDPP board into the junction box and replace the bypass diode. The proposed panel to panel (P2P) for mDPP method is shown in Fig. 11.

Each mDPP converter has current and voltage measurements for its specific PV panel to track the panel's individual maximum

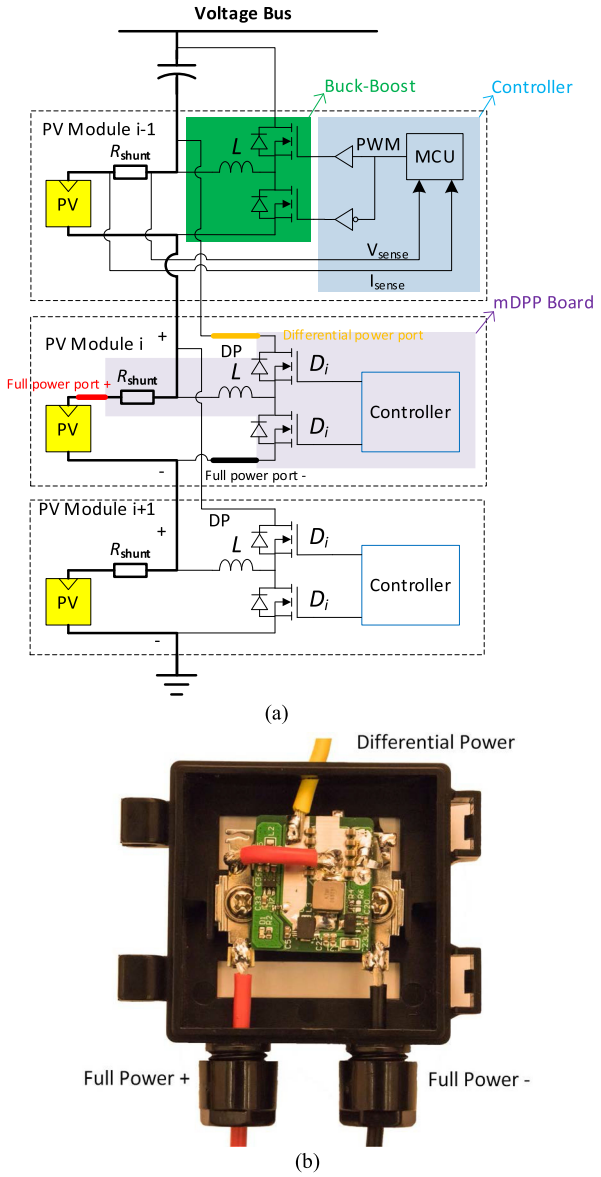

Fig. 11. mDPP hardware design. (a) Modular differential power processing diagram. (b) Photograph of mDPP converter emerged in junction box.

power point. The mDPP converter could also be applied to each PV subpanel to replace the bypass diode individually to gain even better performance. Since the differential power processor usually has low power and voltage rating, it is easy to design a converter with small volume to fit into the junction box for subpanel or panel level solution. Fig. 11(a) shows the block diagram for the simplified connection while Fig. 11(b) shows the photo of the hardware design integrated in the PV junction box.

Each PV panel with its mDPP board in their junction box is called one PV module. In Fig. 11(a), each module will only have three terminals: two main power terminals, "+" for positive terminal and "–" for negative terminal, and one differential power terminal (DP). The positive terminal of ith PV panel is connected to the negative terminal of $(i-1)$th PV panel while the negative terminal is connected to the positive terminal of $(i+1)$th

TABLE I
KEY COMPONENT FOR HARDWARE PROTOTYPE

Component	Description	Quantity
Microcontroller	STM32F334K8	1
Power Module	CSD97394Q4M	1
Inductor	4.7 μH	1
Capacitor (per converter)	10 μF	4
Current Sensor	INA250A2	1
Series capacitor (per string)	100μF	1

PV panel, which connects each PV panel in series as usual. The third terminal, DP terminal, is connected to the positive terminal of $(i-1)$th PV panel. Under this connection the proposed mDPP method is applied for the PV array.

One benefit of the proposed mDPP structure is that it requires only three terminal connections. Previous mDPP methods [22], [33] utilize a total of seven terminal connections per PV Panel: three DPP terminals are required for each submodule converter while two communication ports are used each with two-wire I^2C communication between modules. The proposed method in this article only requires three terminals/wires.

The key components and design detail of the hardware prototype are given in Table I. PWM is running at 230 kHz to eliminate the volume of filter design. The inner voltage loop is running in 1 kHz while the MPPT algorithm is around 10 Hz, which is much faster than the real commercial product. The frequency can be further reduced to eliminate the system cost and energy consumption of the micro controller.

B. Indoor Experiments

In the indoor experiment, a programmable PV panel model is used as in [49]. By applying the same PV panel and program value, the MPPT function and accuracy of proposed control strategy can be validated by comparing the PV voltage and current in the dMPPT and mDPP experiment. Microgrid system usually interfaces a regulated voltage bus with variable loads: the load in Fig. 12 is a dc electronic load in constant voltage mode. Three fully shaded PV panel together with three controllable current sources emulates three different PV panels in [49]. The PV string is connected to a 20 V voltage bus. Fig. 12(b) shows the schematic of the mDPP method. Three distributed mDPP board is applied to each PV panel. As comparison, Fig. 12(c) indicates the connection of the traditional dMPPT method.

In the steady-state experiment, the voltage and the current of each PV panel is measured independently together with the string current I_s and the bus voltage $V_{\rm bus}$. mDPP method and dMPPT method are applied to the same PV panel under the same condition alternatively, taking turns. The test result given in Table II.

PV panel voltage and current of each PV panel is nearly the same in both methods. Small difference existed due to the tracking accuracy of the MPP. But the output power from the PV panel is within certain tracking accuracy. This verifies that both dMPPT and the proposed modular control strategy can track the MPP when it reaches its own steady state.

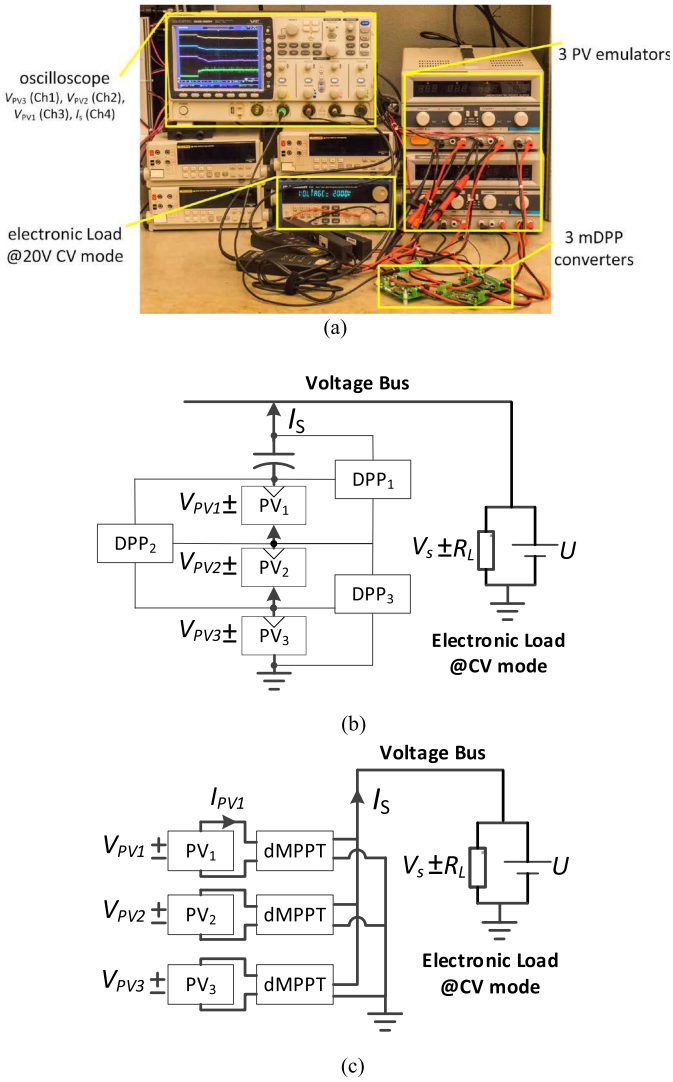

Fig. 12. Indoor experiment. (a) Annotated experimental setup photograph. (b) mDPP experimental schematic. (c) dMPPT experimental schematic.

TABLE II
COMPARISON EXPERIMENT FOR DMPPT AND MDPP METHOD

	dMPPT			mDPP		
	V (V)	I(A)	P(W)	V(V)	I(A)	P(W)
PV11	6.25	2.02	12.63	6.34	1.96	12.43
PV12	6.30	1.81	11.4	6.32	1.77	11.18
PV13	6.44	1.84	11.85	6.40	1.88	12.03
Bus	20.04	1.63	32.67	20.05	1.75	35.12
η_{sys}		91.1%			98.4%	

The system efficiency is defined to represent the ability of the system to harvest much power as well as convert power with less loss. As the MPPT function have been verified, the system efficiency can have a simplified representation as

$$\eta_{sys} = \frac{P_{\rm out}}{\sum P_{{\rm PV}i,{\rm ideal\,MPP}}} = \frac{P_{\rm out}}{\sum P_{{\rm PV}i}}\bigg|_{P_{{\rm PV}i}=P_{\rm MPP}} = \frac{V_s I_s}{\sum_{i=1}^{N} V_{{\rm PV}i} I_{{\rm PV}i}}. \tag{36}$$

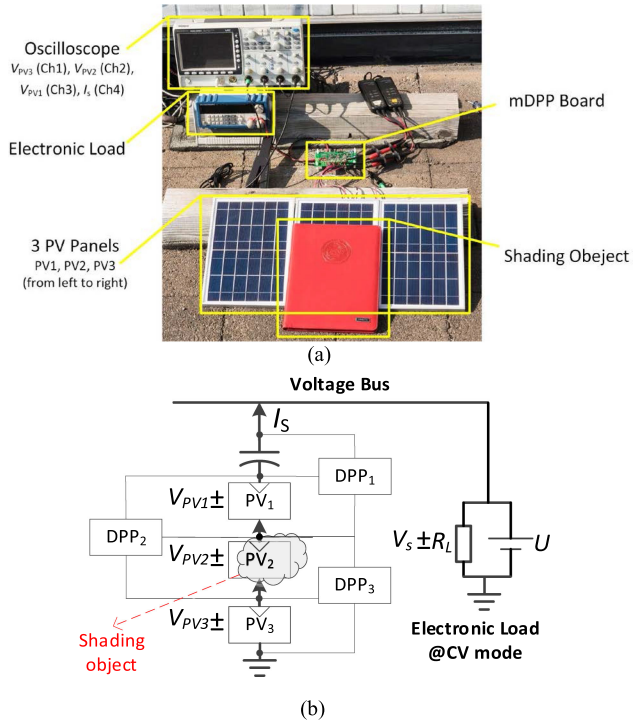

Fig. 13. Outdoor experiment. (a) Annotated experimental setup photo. (b) Outdoor experiment schematic.

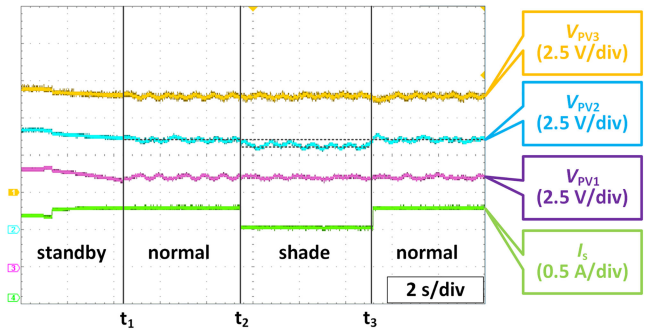

Fig. 14. Waveform of field experiment.

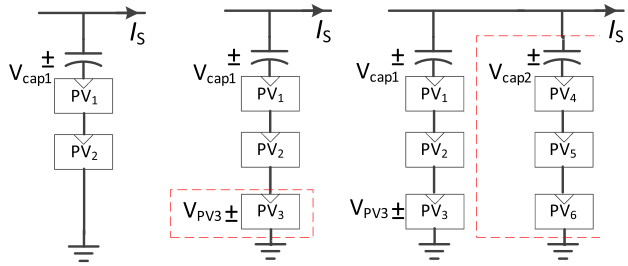

Fig. 15. Simplified schematic of plug and play experiment.

From Table II, dMPPT method shows a 91.1% efficiency compared with proposed method running at 98.4% efficiency. This shows the advantage of the mDPP method. DPP method only processes small amount of power through the converter.

C. Outdoor Shading Experiments

Shading is one of the common challenges faced by the PV system. Outdoor experiment was used to verify the proposed method under real irradiation. The photograph of the experiment is shown in Fig. 13 illustrating three PV panels are connected in series according to the schematic in Fig. 13(b). The voltage across each PV panel and the output current of the string is measured.

With a fixed bus voltage, the string current represents the output power of the whole system. The red notebook in the photo creates partial shading on the PV_2, as shown in the Fig. 13.

The waveform of the field experiment is shown in Fig. 14. The shading object is inserted at time t_2 and then removed at time t_3. The system runs in standby mode before time t_1 and enters soft-start and MPPT function at time t_1. After some adjustment and tracking, three PV panels reach certain steady state value before time t_2, which can be verified as MPP in previous section. At time t_2, a slight drop on the voltage of PV_3 and a larger one on the string current can be observed due to the partial shading of PV_2. Also, it reaches certain steady state value before time t_3. At time t_3, the shading object is removed. Each PV panel voltage and the string current start to recover and finally reach the same level before the time t_2. As discussed in the previous section, the mDPP method can always operate the PV panel in certain steady state which is exactly the MPP of the PV panel. Since the shadow effect only happens for a short period of time, the irradiance and MPP of the PV panels could be considered as constant. This is also verified as all the waveforms remain the same before t_2 and after t_3.

D. Plug and Play Experiment

Following experiment explains the advantage of the plug and play function brought by the proposed control scheme. All six PV panels used in this experiment have similar MPP and are plugged-in at different time with different connection. Fig. 15 shows the connection of PV system when new PV panels in dash line box is plugged in. Note that only the connection of the PV panel connection is shown for simplification while there are corresponding mDPP converters for each panel connected in the manner described previously. Fig. 15(a) shows the original connection, PV_1 and PV_2 are connected in series with a 20 V voltage bus. At time t_1, PV_3 is plugged into the PV string in series with PV_1 and PV_2 as Fig. 15(b). Furthermore, a new PV string with PV_4, PV_5, and PV_6 is added in parallel with previous PV string at time t_3 as in Fig. 15(c).

Fig. 16 shows the waveforms of experimental results. Noted in the Fig. 15, $V_{\rm cap1}$ and $V_{\rm cap2}$ represent the series capacitor voltage. $V_{\rm pv3}$ is the voltage of the PV_3, which is added at time t_1. $I_{\rm s}$ is the total current from the source, which indicates the total output power since a constant voltage load is applied to the system.

Time t_0 to t_1: Only PV_1 and PV_2 are added in the system. $V_{\rm cap1}$ is the voltage difference between two PV panel and the voltage bus, which is roughly 8 V.

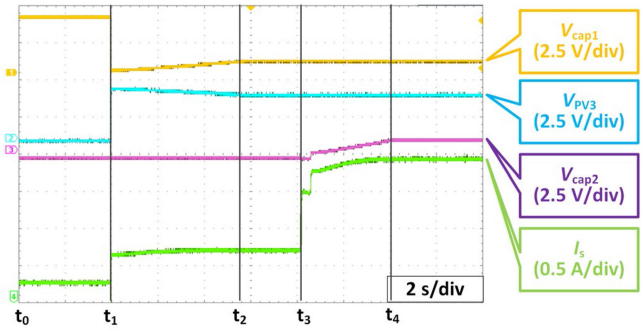

Fig. 16. Waveform of plug and play experiment.

Time t_1 to t_3: PV_3 is added into the system and series capacitor voltage drops to ~1 V at time t_1. V_{cap1} and V_{pv3} keep moving to its steady state when the mDPP converter is looking for the MPP of PV_3. At the same time, the I_s is increasing, which also verifies the direction of moving toward the MPP. At time t_2, the system reaches its steady state, three PV panels operate at its own MPP.

Time After t_3: PV string 2 is added into the system. Its corresponding mDPP converters start to operate PV panels toward its MPP. The V_{cap2} reaches its steady state at time t_4 while the output current reaches its maximum value.

In this experiment, PV system with mDPP has successfully demonstrated the features of operating at MPP when new panels are added. Modularity has been achieved without any modification of the existed system.

VIII. Conclusion

In this article, we proposed the detailed methods to realize the PV2PV and P2P transfer method for the mDPP concept to solve the modularity and scalability problem. The series capacitor, which is used as a "virtual PV panel," can absorb any voltage difference between the PV string and the voltage bus. This concept yields the high levels of system efficiency and plug and play function. A central converter is no longer needed for MPPT, which is typical of other DPP methods. This eliminates the power losses associated with an full power processing converter. No communication is required between the panels and true distributed control strategy is proposed. This enables the modular plug and play capability and simplified wire connections. Simple PI controllers are demonstrated to be stable and allow MPPT operation for each subpanel. Since the controllers are based on linearized models, as well as a "slow response" assumption, the stability results are only small signal (local). But this is typical of power converter controllers. Robustness to aging, equivalent series resistance (ESR), panel mismatch over time must still be investigated. However, simulations, indoor experiments, and small-scale proof-of-concept outdoor experiments verify the plug and play operation, and even higher than 98% of efficiency is achieved.

Appendix

This appendix demonstrates that all the $a_{ii} < 0$ in (12) so that the local stability in Section IV can be proven

$$a_{ii} = \left.\frac{\partial f_i}{\partial d_i(t)}\right|_{\mathbf{D}} = \left.\frac{\partial\left(V_{\text{bus}} \times \frac{\prod_{j=1}^{i}\frac{1-d_j(t)}{d_j(t)}}{(1+\sum_{m=1}^{N}\prod_{j=1}^{m}\frac{1-d_j(t)}{d_j(t)})}\right)}{\partial d_i}\right|_{\mathbf{D}}.$$

$$= V_{\text{bus}} \times \left.\frac{\partial\left(\frac{\left(\frac{1}{d_1}-1\right)\left(\frac{1}{d_2}-1\right)\cdots\left(\frac{1}{d_i}-1\right)}{1+\left(\frac{1}{d_1}-1\right)+\left(\frac{1}{d_1}-1\right)\left(\frac{1}{d_2}-1\right)+\cdots+\left(\frac{1}{d_1}-1\right)\left(\frac{1}{d_2}-1\right)\cdots\left(\frac{1}{d_N}-1\right)}\right)}{\partial d_i}\right|_{\mathbf{D}}.$$

Define

$$\prod_{j=1}^{i}\frac{1-d_j(t)}{d_j(t)} = \left(\frac{1}{d_1}-1\right)\left(\frac{1}{d_2}-1\right)\cdots\left(\frac{1}{d_i}-1\right) = \beta_i$$

which for any $d_i \in (0,1)$, will have each $\beta_i > 0$. Furthermore, define Δ as

$$1 + \sum_{m=1}^{N}\prod_{j=1}^{m}\frac{1-d_j(t)}{d_j(t)} = 1 + \beta_1 + \beta_2 + \cdots + \beta_N = \Delta$$

which also will satisfy $\Delta > 0$ since $\beta_j > 0$ for any $j = 1, 2, \ldots, N$. Rewriting a_{ii} leads to, shown at the bottom of the page which simplifies to become

$$a_{ii} = V_{\text{bus}} \times \left.\frac{\left[\beta_{i-1}\cdot\left(-\frac{1}{d_i^2}\right)\right]\cdot\left[\Delta - (\beta_i + \beta_{i+1} + \cdots \beta_N)\right]}{\Delta^2}\right|_{\mathbf{D}}$$

$$= V_{\text{bus}} \times \left.\frac{\left[\beta_{i-1}\cdot\left(-\frac{1}{d_i^2}\right)\right]\cdot\left[1 + \beta_1 + \beta_2 + \cdots + \beta_{i-1}\right]}{\Delta^2}\right|_{\mathbf{D}}.$$

Since $\beta_j > 0$, and $d_j > 0$ for any $j = 1, 2, \ldots, N$, this demonstrates that $a_{ii} < 0$.

$$a_{ii} = V_{\text{bus}} \times \left.\frac{\left[\beta_{i-1}\cdot\left(-\frac{1}{d_i^2}\right)\right]\cdot\Delta - \left[\beta_{i-1}\cdot\left(-\frac{1}{d_i^2}\right) + \beta_{i-1}\cdot\left(-\frac{1}{d_i^2}\right)\left(\frac{1}{d_{i+1}}-1\right) + \cdots + \beta_{i-1}\cdot\left(-\frac{1}{d_i^2}\right)\prod_{j=i+1}^{N}\left(\frac{1}{d_j}-1\right)\right]\beta_i}{\Delta^2}\right|_{\mathbf{D}}$$

$$= V_{\text{bus}} \times \left.\frac{\left[\beta_{i-1}\cdot\left(-\frac{1}{d_i^2}\right)\right]\cdot\left[\Delta - \left(1 + \left(\frac{1}{d_{i+1}}-1\right) + \left(\frac{1}{d_{i+1}}-1\right)\left(\frac{1}{d_{i+2}}-1\right) + \cdots + \prod_{j=i+1}^{N}\left(\frac{1}{d_j}-1\right)\right)\beta_i\right]}{\Delta^2}\right|_{\mathbf{D}}$$

Similarly, a_{ij} can also be deduced as follows:

$$a_{ij} = \left.\frac{\partial f_i}{\partial d_j(t)}\right|_{\mathbf{D}} = \left.\frac{\partial\left(V_{bus}\times\frac{\prod_{k=1}^{i}\frac{1-d_k(t)}{d_k(t)}}{(1+\sum_{m=1}^{N}\prod_{k=1}^{m}\frac{1-d_k(t)}{d_k(t)})}\right)}{\partial d_j}\right|_{\mathbf{D}}$$

$$= V_{\mathrm{bus}}\left.\frac{\partial\left(\frac{\left(\frac{1}{d_1}-1\right)\left(\frac{1}{d_2}-1\right)\cdots\left(\frac{1}{d_i}-1\right)}{1+\left(\frac{1}{d_1}-1\right)+\left(\frac{1}{d_1}-1\right)\left(\frac{1}{d_2}-1\right)+\cdots+\left(\frac{1}{d_1}-1\right)\left(\frac{1}{d_2}-1\right)\cdots\left(\frac{1}{d_N}-1\right)}\right)}{\partial d_j}\right|_{\mathbf{D}}.$$

Then

$$f_i(\mathbf{d}(t))=\frac{\beta_i}{\sum_{k=1}^{N}\beta_k}$$

$$a_{ij} = \left.\frac{\partial f_i}{\partial d_j(t)}\right|_{\mathbf{D}} = \left.\frac{\frac{\partial\beta_i}{\partial d_j}\cdot\sum_{k=1}^{N}\beta_k - \frac{\partial(\sum_{k=1}^{N}\beta_k)}{\partial d_j}\cdot\beta_i}{\left(\sum_{k=1}^{N}\beta_k\right)^2}\right|_{\mathbf{D}}.$$

The left part in numerator is

$$\frac{\partial\beta_i}{\partial d_j}\cdot\sum_{k=1}^{N}\beta_k = \left(-\frac{1}{d_j^2}\right)\frac{\beta_i}{\frac{1}{d_j}-1}\cdot\sum_{k=1}^{N}\beta_k.$$

The right part in numerator is

$$\frac{\partial(\sum_{k=1}^{N}\beta_k)}{\partial d_j}\cdot\beta_i = \left(-\frac{1}{d_j^2}\right)\frac{\beta_i}{\frac{1}{d_j}-1}\cdot\sum_{k=j}^{N}\beta_k.$$

Then

$$a_{ij} = \left.\frac{\partial f_i}{\partial d_j(t)}\right|_{\mathbf{D}} = \left.\frac{\left(-\frac{1}{d_j^2}\right)\frac{\beta_i}{\frac{1}{d_j}-1}\cdot\sum_{k=1}^{j-1}\beta_k}{\left(\sum_{k=1}^{N}\beta_k\right)^2}\right|_{\mathbf{D}}.$$

REFERENCES

[1] L. Chen, A. Amirahmadi, Q. Zhang, N. Kutkut, and I. Batarseh, "Design and implementation of three-phase two-stage grid-connected module integrated converter," *IEEE Trans. Power Electron.*, vol. 29, no. 8, pp. 3881–3892, Aug. 2014.

[2] Q. Zhang *et al.*, "A center point iteration MPPT method with application on the frequency-modulated LLC microinverter," *IEEE Trans. Power Electron.*, vol. 29, no. 3, pp. 1262–1274, Mar. 2014.

[3] B. J. Pierquet and D. J. Perreault, "A single-phase photovoltaic inverter topology with a series-connected energy buffer," *IEEE Trans. Power Electron.*, vol. 28, no. 10, pp. 4603–4611, Oct. 2013.

[4] W. Cha, Y. Cho, J. Kwon, and B. Kwon, "Highly efficient microinverter with soft-switching step-up converter and single-switch-modulation inverter," *IEEE Trans. Ind. Electron.*, vol. 62, no. 6, pp. 3516–3523, Jun. 2015.

[5] X. Zhang, M. Amirabadi, and B. Lehman, "A long-lifespan single-phase single-stage multi-module inverter for PV application," in *Proc. 44th Annu. Conf. IEEE Ind. Electron. Soc.*, 2018, pp. 6103–6109.

[6] L. F. L. Villa, T. Ho, J. Crebier, and B. Raison, "A power electronics equalizer application for partially shaded photovoltaic modules," *IEEE Trans. Ind. Electron.*, vol. 60, no. 3, pp. 1179–1190, Mar. 2013.

[7] Y. Li, Y. Zheng, S. Sheng, B. Scandrett, and B. Lehman, "Modular subpanel photovoltaic converter system: Analysis and control," in *Proc. IEEE Appl. Power Electron. Conf. Expo.*, 2016, pp. 417–423.

[8] Y. Zheng, Y. Li, S. Sheng, B. Scandrett, and B. Lehman, "Distributed control for modular plug-and-play subpanel photovoltaic converter system," in *Proc. IEEE Appl. Power Electron. Conf. Expo.*, 2017, pp. 1267–1271.

[9] C. Liu, D. Li, Y. Zheng, and B. Lehman, "Modular differential power processing (mDPP)," in *Proc. IEEE 18th Workshop Control Model. Power Electron.*, 2017, pp. 1–7.

[10] C. Liu, Y. Zheng, D. Li, and B. Lehman, "Distributed MPPT for modular differential power processing in scalable photovoltaic system," in *Proc. IEEE Appl. Power Electron. Conf. Expo.*, 2018, pp. 1098–1103.

[11] M. Das and V. Agarwal, "Design and analysis of a high-efficiency DC–DC converter with soft switching capability for renewable energy applications requiring high voltage gain," *IEEE Trans. Ind. Electron.*, vol. 63, no. 5, pp. 2936–2944, May 2016.

[12] G. Zhang, B. Zhang, Z. Li, D. Qiu, L. Yang, and W. A. Halang, "A 3-Z-network boost converter," *IEEE Trans. Ind. Electron.*, vol. 62, no. 1, pp. 278–288, Jan. 2015.

[13] G. Wu, X. Ruan, and Z. Ye, "Nonisolated high step-up DC–DC converters adopting switched-capacitor cell," *IEEE Trans. Ind. Electron.*, vol. 62, no. 1, pp. 383–393, Jan. 2015.

[14] T. Shimizu, M. Hirakata, T. Kamezawa, and H. Watanabe, "Generation control circuit for photovoltaic modules," *IEEE Trans. Power Electron.*, vol. 16, no. 3, pp. 293–300, May 2001.

[15] P. S. Shenoy, K. A. Kim, B. B. Johnson, and P. T. Krein, "Differential power processing for increased energy production and reliability of photovoltaic systems," *IEEE Trans. Power Electron.*, vol. 28, no. 6, pp. 2968–2979, Jun. 2013.

[16] P. S. Shenoy and P. T. Krein, "Differential power processing for DC systems," *IEEE Trans. Power Electron.*, vol. 28, no. 4, pp. 1795–1806, Apr. 2013.

[17] E. Candan, D. Heeger, P. S. Shenoy, and R. C. N. Pilawa-Podgurski, "A series-stacked power delivery architecture with hot-swapping for high-efficiency data centers," in *Proc. IEEE Energy Convers. Congr. Expo.*, 2015, pp. 571–578.

[18] E. Candan, D. Heeger, P. S. Shenoy, and R. C. N. Pilawa-Podgurski, "Hot-swapping analysis and implementation of series-stacked server power delivery architectures," *IEEE Trans. Power Electron.*, vol. 32, no. 10, pp. 8071–8088, Oct. 2017.

[19] E. Candan, P. S. Shenoy, and R. C. N. Pilawa-Podgurski, "A series-stacked power delivery architecture with isolated differential power conversion for data centers," *IEEE Trans. Power Electron.*, vol. 31, no. 5, pp. 3690–3703, May 2016.

[20] Y. Levron, D. R. Clement, B. Choi, C. Olalla, and D. Maksimovic, "Control of submodule integrated converters in the isolated-port differential power-processing photovoltaic architecture," *IEEE J. Emerg. Sel. Topics Power Electron.*, vol. 2, no. 4, pp. 821–832, Dec. 2014.

[21] S. Qin, S. T. Cady, A. D. Domínguez-García, and R. C. N. Pilawa-Podgurski, "A distributed approach to MPPT for PV sub-module differential power processing," in *Proc. IEEE Energy Convers. Congr. Expo.*, 2013, pp. 2778–2785.

[22] S. Qin and R. C. N. Pilawa-Podgurski, "Sub-module differential power processing for photovoltaic applications," in *Proc. 28th Annu. IEEE Appl. Power Electron. Conf. Expo.*, 2013, pp. 101–108.

[23] K. Sun, Z. Qiu, H. Wu, and Y. Xing, "Evaluation on high-efficiency thermoelectric generation systems based on differential power processing," *IEEE Trans. Ind. Electron.*, vol. 65, no. 1, pp. 699–708, Jan. 2018.

[24] F. Wang, T. Zhu, F. Zhuo, and H. Yi, "An improved submodule differential power processing-based PV system with flexible multi-MPPT control," *IEEE J. Emerg. Sel. Topics Power Electron.*, vol. 6, no. 1, pp. 94–102, Mar. 2018.

[25] N. B. Kumar and M. K. N. Mounika, "Implementation of differential power processing to optimize the solar power generation," in *Proc. Int. Conf. Current Trends Toward Converging Technol.*, 2018, pp. 1–7.

[26] Y. T. Jeon, H. Lee, K. A. Kim, and J. H. Park, "Least power point tracking method for photovoltaic differential power processing systems," *IEEE Trans. Power Electron.*, vol. 32, no. 3, pp. 1941–1951, Mar. 2017.

[27] Y. Jeon and J. Park, "Unit-minimum least power point tracking for the optimization of photovoltaic differential power processing systems," *IEEE Trans. Power Electron.*, vol. 34, no. 1, pp. 311–324, Jan. 2019.

[28] G. Chu and H. Wen, "Design and optimization of PV-isolated-port photovoltaic differential power porcessing system," in *Proc. IEEE Int. Conf. Power Electron. Drives Energy Syst.*, 2018, pp. 1–6.

[29] P. Wang, Y. Chen, J. Yuan, R. G. C. N. Pilawa-Podgurski, and M. G. Chen, "Differential power processing for ultra-efficient data storage," *IEEE Trans. Power Electron.*, vol. 36, no. 4, pp. 4269–4286, Apr. 2021.

[30] M. S. Zaman *et al.*, "A cell-level differential power processing IC for concentrating-PV systems with bidirectional hysteretic current-mode control and closed-loop frequency regulation," *IEEE Trans. Power Electron.*, vol. 30, no. 12, pp. 7230–7244, Dec. 2015.

[31] C. Olalla, C. Deline, D. Clement, Y. Levron, M. Rodriguez, and D. Maksimovic, "Performance of power-limited differential power processing architectures in mismatched PV systems," *IEEE Trans. Power Electron.*, vol. 30, no. 2, pp. 618–631, Feb. 2015.
[32] S. Qin, C. B. Barth, and R. C. N. Pilawa-Podgurski, "Enhancing microinverter energy capture with submodule differential power processing," *IEEE Trans. Power Electron.*, vol. 31, no. 5, pp. 3575–3585, May 2016.
[33] S. Qin, S. T. Cady, A. D. Domínguez-García, and R. C. N. Pilawa-Podgurski, "A distributed approach to maximum power point tracking for photovoltaic submodule differential power processing," *IEEE Trans. Power Electron.*, vol. 30, no. 4, pp. 2024–2040, Apr. 2015.
[34] M. O. Badawy, S. M. Bose, and Y. Sozer, "A novel differential power processing architecture for a partially shaded PV string using distributed control," *IEEE Trans. Ind. Appl.*, vol. 57, no. 2, pp. 1725–1735, Mar./Apr. 2021, doi: 10.1109/TIA.2020.3046430.
[35] G. Chu H. Wen, Y. Hu, L. Jiang, Y. Yang, and Y. Wang, "Low-complexity power-balancing-point based optimization for photovoltaic differential power processing," *IEEE Trans. Power Electron.*, vol. 35, no. 10, pp. 10306–10322, Oct. 2020.
[36] G. Chu, H. Wen, Y. Yang, and Y. Wang, "Elimination of photovoltaic mismatching with improved submodule differential power processing," *IEEE Trans. Ind. Electron.*, vol. 67, no. 4, pp. 2822–2833, Apr. 2020.
[37] H. Jeong, H.-T. Cho, T. Kim, Y.-C. Liu, and K. A. Kim, "A scalable unit differential power processing system design for photovoltaic applications," in *Proc. IEEE 19th Workshop Control Model. Power Electron.*, 2018, pp. 1–8.
[38] P. Wang, Y. Chen, P. Kushima, Y. Elasser, M. Liu, and M. Chen, "A 99.7% efficient 300 W hard disk drive storage server with multiport AC-coupled differential power processing (MAC-DPP) architecture," in *Proc. IEEE Energy Convers. Congr. Expo.*, 2019, pp. 5124–5131.
[39] M. S. Agamy *et al.*, "An efficient partial power processing DC/DC converter for distributed PV architectures," *IEEE Trans. Power Electron.*, vol. 29, no. 2, pp. 674–686, Feb. 2014.
[40] T. Suntio and A. Kuperman, "Comments on 'an efficient partial power processing DC/DC converter for distributed PV architectures'," *IEEE Trans. Power Electron.*, vol. 30, no. 4, pp. 2372–2372, Apr. 2015.
[41] L. Lin, J. Zhang, and S. Shao, "Differential power processing architecture with virtual port connected in series and MPPT in submodule level," *IEEE Access*, vol. 8, pp. 137897–137909, 2020.
[42] K. A. Kim, P. S. Shenoy, and P. T. Krein, "Converter rating analysis for photovoltaic differential power processing systems," *IEEE Trans. Power Electron.*, vol. 30, no. 4, pp. 1987–1997, Apr. 2015.
[43] Y. Gu, X. Xiang, W. Li, and X. He, "Mode-adaptive decentralized control for renewable DC microgrid with enhanced reliability and flexibility," *IEEE Trans. Power Electron.*, vol. 29, no. 9, pp. 5072–5080, Sep. 2014.
[44] P. Prabhakaran, Y. Goyal, and V. Agarwal, "Novel nonlinear droop control techniques to overcome the load sharing and voltage regulation issues in DC microgrid," *IEEE Trans. Power Electron.*, vol. 33, no. 5, pp. 4477–4487, May 2018.
[45] S. Peyghami, P. Davari, H. Mokhtari, P. C. Loh, and F. Blaabjerg, "Synchronverter-enabled DC power sharing approach for LVDC microgrids," *IEEE Trans. Power Electron.*, vol. 32, no. 10, pp. 8089–8099, Oct. 2018.
[46] M. Kasper, S. Herden, D. Bortis, and J. W. Kolar, "Impact of PV string shading conditions on panel voltage equalizing converters and optimization of a single converter system with overcurrent protection," in *Proc. 16th Eur. Conf. Power Electron. Appl.*, 2014, pp. 1–10.
[47] L. Ciani, M. Catelani, E. A. Carnevale, L. Donati, and M. Bruzzi, "Evaluation of the aging process of dye-sensitized solar cells under different stress conditions," *IEEE Trans. Instrum. Meas.*, vol. 64, no. 5, pp. 1179–1187, May 2015.
[48] Y. Hu, J. Zhang, J. Wu, W. Cao, G. Y. Tian, and J. L. Kirtley, "Efficiency improvement of nonuniformly aged PV arrays," *IEEE Trans. Power Electron.*, vol. 32, no. 2, pp. 1124–1137, Feb. 2017.
[49] S. Qin, K. A. Kim, and R. C. N. Pilawa-Podgurski, "Laboratory emulation of a photovoltaic module for controllable insolation and realistic dynamic performance," in *Proc. IEEE Power Energy Conf. Illinois*, 2013, pp. 23–29.

Chang Liu (Student Member, IEEE) received the B.S.E.E. degree from Southwest Jiaotong University, Chengdu, China, in 2016, and the M.S.E.E. degree in 2019 from Northeastern University, Boston, MA, USA, where he is currently working toward the Ph.D. degree in electrical engineering.

His research interests include PV dc–dc converters, differential power processing.

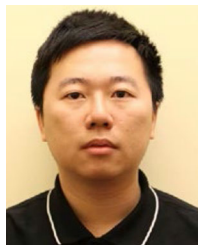

Yue Zheng (Student Member, IEEE) received the B.S.E.E. degree from Tsinghua University, Beijing, China, in 2012, and the M.S.E.E. and Ph.D. degrees in electrical engineering from Northeastern University, Boston, MA, USA, in 2015 and 2021, respectively.

His research interests include PWM algorithm, SD card flash memory, LED driver, dc–dc converters paralleling for weak dc grid, and wireless charging.

Brad Lehman (Fellow, IEEE) is a Professor with the Department of Electrical and Computer Engineering, Northeastern University, Boston, MA, USA. He was an Editor-in-Chief for the IEEE TRANSACTIONS ON POWER ELECTRONICS from 2013 to2018 and is currently the Vice President for products in the IEEE Power Electronics Society (PELS). He has been listed in the inaugural edition of the book "The 300 Best Professors," Princeton Review, 2012. Before becoming a Professor, he was the Head of swimming and diving coach with the Georgia Institute of Technology, where he also earned his Ph.D.E.E. in 1992. His research interests include power electronics and controls, with applications to solar energy, LED lighting, battery energy management systems, and reliability.

Dr. Lehman has been the recipient of the 2015 IEEE (PELS) Modeling and Control Technical Achievement Award, a 2016 IEEE Standards Medallion, the 2018 IEEE Award for Achievement in Power Electronics Standards, and the 2019 IEEE PELS Harry A. Owen, Jr. Distinguished Service Award.